Accurate estimation of temperatures in a cryogenic space cooled by a Stirling cryocooler

Dmitry Smirnov*

Thermal Motors LLC, Moscow, Russia

Henni Ouerdane

Skolkovo Institute of Science and Technology, Moscow, Russia

Abstract

The experimental analysis of cryogenic chambers coupled with Stirling cryocoolers has received scant attention in the research literature. This work provides a novel contribution by developing and experimentally validating an analytical model of the coupling to predict temperatures in the system. The paper unifies the Stirling cryocooler equation previously derived by Otaka *et al.* and the thermal-electrical analogy for the chamber. The analytical formula predicts steady-state temperatures in the chamber as a function of the system's controllable design and operational parameters. The model was validated with experimental data from 15 tests of an alpha-type Stirling cryocooler coupled with a thermal chamber. The resulting model showed an accurate prediction of temperatures with an average coefficient of variance of 5%, mean biased error of 2%, and R^2 value of 0.95. The findings are relevant because of the urgent need to learn how to control cryogenic spaces using electricity-based systems. Such spaces will be of high significance in the future because advanced solutions and products in biomedicine, electronics, computing and other fields use cryogenic spaces.

Keywords: Stirling cryocooler, cryogenic chamber, thermodynamic modelling, cryogenic temperature measurements.

*Corresponding author, dmitry.smirnov@thermalmotors.com,

Dmitry Smirnov: ORCID: 0000-0003-4867-9000

Henni Ouerdane, ORCID: 0000-0002-1914-0244

I Introduction

How to predict the temperature distribution in a closed thermal chamber cooled by a Stirling cryocooler? With the advent of advanced technologies in biomedicine, high-temperature superconductor electronics, cryo-CMOS devices, and even quantum computing, this question has become timely as many inventions and discoveries require controlling, manipulating, and otherwise experimenting with cryogenic environments using electricity and engineering tools, such as cryocoolers. Predicting and controlling the temperature in these environments with the design and operation parameters of a cryocooler and thermal chamber is a significant practical problem.

The research that focuses on the interaction between the cryocooler and the cooling environment is scarce. Studies by Oguz and Ozkadi (2002, 2000), Kwon and Berchowitz (2003) or Otaka *et al.* (2008), on a Stirling cryocooler connected to a thermal chamber or a refrigeration cabinet provided measurement data on the cooling temperatures and performance as a function of heating load, cryocooler input energy or refrigerant type. These experiments demonstrate what happens in a thermal chamber when particular types of cryocoolers were selected and operated at different input energies. However, they do not offer analytical models that relate cooling temperatures with operational and design parameters of the cryocooler and thermal chamber. In addition, the results are only relevant for particular cryocooler designs. Future progress in the field should transform empirical results into a form applicable to analyzing cryocoolers with different design variables.

Otaka *et al.* (2002), in an earlier work, proposed and empirically confirmed an analytical approach to relate the design and operational parameters of a cryocooler to the cooling capacity. This was the first important step towards the prediction of temperatures inside a thermal chamber. In the present work, we go further and deeper in scope as it is necessary to identify an appropriate theoretical concept that can describe the thermal state in the chamber in a physically transparent fashion. We aim to unify and experimentally validate a joint model based on the Otaka's Stirling cryocooler model and the model for a thermal chamber.

The article is organized as follows. The following section discusses the main assumptions, works out the analytical relations and describes the experimental methodology. Section III shows the results of experimental tests of the cryocooler. Section IV discusses the results, limitations and future work. Section V concludes on the findings.

II Methodology

Several assumptions are in order before selecting a formal description of the heat transfer between a cryocooler and the chamber. To simplify the problem, we consider steady-state conditions when temperature fluctuations and variations are negligible. This means that non-equilibrium or transient processes are not considered. It has been shown elsewhere that in normal conditions, transient states continue for dozens of minutes for the cooldown from the room conditions (Oguz & Ozkadi, 2000; Djetel-Gothe *et al.*, 2020), or several minutes for changes inside the cryocooler during the operation (Smirnov *et al.*, 2019). In other words, under a constant heating load, a cryocooler finds an equilibrium with the thermal chamber fast enough. In general, a cryocooler operates in a steady-state. Therefore, this assumption is valid. However, if a cryocooler is applied to a varying heating load, this assumption would no longer be valid. An example could be the cooling of a cryo-CMOS computer processor, where the integrated circuit is a varying heat source.

The second assumption is that thermal radiation is absent. Presumably, the cryogenic temperatures of the thermal chamber walls would prevent high radiative powers. This can be checked using the Stefan–Boltzmann law. A grey body with emissivity $\varepsilon = 0.5$, temperature

$T = 80\,\mathrm{K}$, and total surface of $A = 0.25\,\mathrm{m}^2$ would radiate with the power $P = 0.3\,\mathrm{W}$. These conditions represent a thermal chamber with a shoebox-size with internal walls made of stainless steel 301. For simplicity, let us assume that the thermal radiation flow from the cryocooler to the chamber wall is negligible. The cryocooler surface is several times smaller, and the temperature is dozens of kelvins lower than that in the chamber. The chamber's thermal radiation power starting from 5 W can be regarded as significant, considering that the expected cooling capacities of a medium-size Stirling cryocooler start from 50 W. Such a radiative power would result from wall temperatures of 162 K, which is a relatively low temperature and might occur during the operation. Although we assumed that thermal radiation could be neglected initially, we should be cautious with this assumption, subject to temperatures and material emissivity of chamber walls.

The third assumption is that the chamber's external wall temperature is equal to the room temperature. This is a reasonable assumption if a room is large enough, which is very often the case.

The fourth assumption is that there is a movement of gas in the thermal chamber driven by a fan. This assumption was used for two reasons. First, it follows from practical considerations as the efficiency of the forced convection is higher. Objects are cooled faster using the forced flow of gas. Second, forced convection measurements and modelling are more manageable because of the resulting homogeneity of the thermal properties in the chamber. This assumption might not be valid if the cooling object could be in direct contact with the cryocooler's cold head, and the chamber is isolated with the vacuum.

With neglected thermal radiation, the heat transfer between the cryocooler and a thermal chamber and the thermal chamber and environment consists of two heat transfer mechanisms. Heat flows through the conduction within the chamber's walls and the forced heat convection between the internal wall and the cryocooler. In the most general case, the conduction is described by the differential form of Fourier's law $\bar{q} = -k\nabla T$. Here $\bar{q} = f\left(\bar{x},t\right)$ is the direction and magnitude of the heat flow as a function of space and time, k is the thermal conductivity, and $\nabla T = f\left(\bar{x},t\right)$ is the temperature gradient as a function of space and time. As we assumed a steady state, the time variable t cancels. The heat flow for forced convection is calculated in a general case as $\bar{q} = -k\nabla T + \rho i \bar{w}$, where the first term describes the gas molecular conduction and the second term characterizes the transfer of enthalpy i by the gas flow with density ρ and velocity $\bar{w}$.

A practical approach to go from differential equations to a simple empirical relation is to define the heat transfer in the gas flow using the empirical law of Newton-Richmann, $q = \alpha \cdot \Delta T$, where α is an empirical constant. This method allows us to use the *thermal-electrical analogy* to describe the thermal state in the chamber. The approach is common in the heat transfer literature and simple enough for the first-order analysis (Lienhard & Lienhard, 2001, p. 70).

Using this approach, we formulate the two main objectives of the present work:

1) To develop a unified numerical model for the system “Stirling cryocooler—Thermal chamber” to predict the steady-state temperature of the gas in the chamber.

2) To carry out real experimental tests to collect temperature data and validate the prediction accuracy of a developed analytical relation.

The following section defines the object and boundaries of the study.

II.1 Object of analysis

The object of analysis is the thermo-mechanical system “Stirling cryocooler—Thermal chamber” (hereafter – the system), shown in Fig. 1a. In the figure, T_{atm} is the atmospheric temperature (K), T_{c} is the cryocooler temperature (K), $T_{g}^{st.s}$ is the steady-state gas temperature in the thermal chamber (hereafter – TC) (K). An electromotor drives the Stirling cryocooler (hereafter – SC). The latter converts input mechanical work into cooling capacity and cools the gas in the TC. The heat transfer occurs due to forced convection initiated by the gas and the air circulated in the chamber by the electrical fan.

Figure 1b depicts the thermo-electrical analogy of the system. We used this analogy to model the thermal balance in the chamber. In Fig. 1b, q_{c} is the cooling capacity of the SC (W), q_{L} is the sum of all parasite heat leaks from the atmospheric environment (W), $R_{atm\text{-}g}$ is total thermal resistance of the system "atmosphere-gas" ($K \cdot W^{-1}$) and $R_{g\text{-}R}$ is the thermal resistance of the system "gas-SC" ($K \cdot W^{-1}$). Table 1 lists key operational, geometrical and thermal parameters of system used in the analysis.

II.2 Steady-state gas temperature in the thermal chamber

Here, we derive an expression for the steady-state temperature of the gas in the chamber as a function of cryocooler control parameters and environment conditions.

II.2.1 Cooling capacity of the Stirling cryocooler

In Eq. 1, which was adapted from the experimental work of Otaka *et al.* (2002), S_{c} is a design configuration constant (cm^{3}) defined below (2), f is the frequency of the cycle (Hz), p is charge pressure (MPa), T_{c} is refrigeration temperature (K) and T_{r} is the temperature of the cryocooler's radiator (K).

$$q_{c} = S_{c} \cdot \Theta \cdot f \cdot p \cdot \frac{T_{c}}{T_{r}} \tag{1}$$

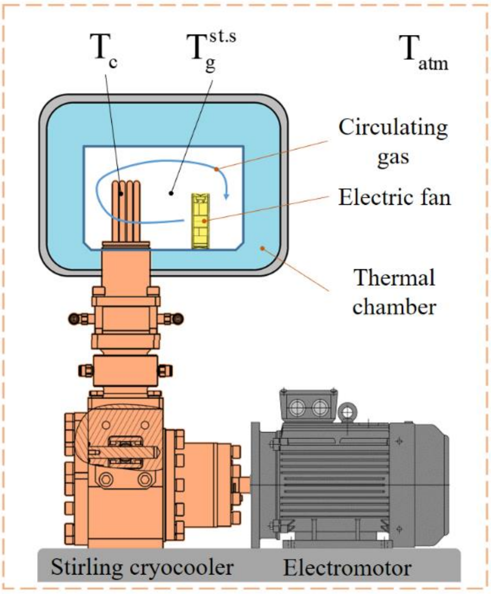

a)

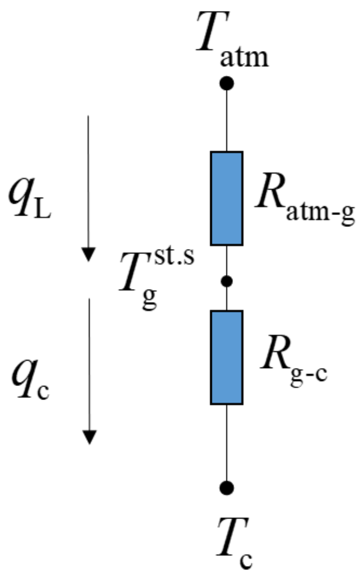

b)

Fig. 1. The system "Stirling cryocooler–Thermal chamber": a) principal diagram with key elements b) Thermal-electrical analogy.

Table 1. Characteristics of the Stirling cryocooler and the thermal chamber used in the analysis.

Stirling cryocooler	
Cooling capacity, q_c	50 W
Refrigeration temperature, T_c	123 K
Radiator temperature, T_r	287 K
Working fluid	Helium
Width × height × depth	262 × 474 × 205 mm
Charge pressure, p	2.5 MPa
Shaft frequency, f	9 Hz
Cold surface area, A_c	$0.024\ \mathrm{m^2}$
Thermal chamber	
Circulating gas	Air
External width × height ×depth	330 × 250 × 425 mm
Internal width × height ×depth	225 × 135 × 275 mm
External surface area	$0.724\ \mathrm{m^2}$
Internal surface area	$0.259\ \mathrm{m^2}$
Heat conductance of the wall	$0.040\ \mathrm{W \cdot m^{-1} \cdot K^{-1}}$

The parameter Θ was introduced by Otaka and co-workers as a *constant* that contains "the effects of phase-difference temperature ratio, volume ratio, and dead volume ratio". We hereafter refer to it as the Otaka number. The parameter S_c in Eq. (1) reads:

$$S_{\mathrm{c}} = V_{\mathrm{e}} \frac{\kappa \cdot \sin\varphi}{\xi} \cdot (\kappa + 1) \tag{2}$$

Where V_{e} is expansion volume (cm^3), κ the ratio between the compression and expansion volumes, φ is the phase difference between the moving compression and expansion pistons, ξ is the dead volume ratio between the total dead volume and the expansion volume. For this study the parameter S_c is a constant number (Table 2) due to a fixed design of the experimental SC.

Table 2. Design parameters of the Stirling cryocooler.

Parameter	**Value**
Expansion volume, V_e, cm^3	60
Volume ratio, κ	1
Phase difference, φ	90
Dead volume ratio, ξ	1.33
Design configuration constant, S_{c}, cm^3	90.2 (calculated, eq. 2)

Equations 1 and 2 define the relationship between the cooling capacity of the SC and its design and control parameters. The advantage of this method is simplicity. The drawback is the need to experimentally obtain the constant Θ and having $T_{\mathrm{c}}(\Theta)$ as an input parameter. Numerical calculation of Θ is possible but difficult because the Otaka number is an aggregate characteristic of the cryocooler performance. It depends on the specific design of the refrigeration system and to the authors' knowledge, no study suggests a method to calculate it numerically. In this work, we obtained Θ with three preliminary tests of the cryocooler and measured all parameters in Eq. 1 except the Otaka number, which was then calculated from the relation. The temperature of the cryocooler is not an independent variable in Eq. 1. This poses additional (unnecessary) challenges. The following three subsections focus on the derivation of the gas temperature in the chamber with factoring out the cryocooler temperature.

II.2.2 Steady-state for the cryocooler and the gas in the thermal chamber

$$q_{\mathrm{c}} = \frac{T_{\mathrm{g}} - T_{\mathrm{c}}}{R_{\text{g-c}}} = \frac{T_{\mathrm{g}} - T_{\mathrm{c}}}{1/\left(h_{\text{g-c}} \cdot A_{\mathrm{c}}\right)} \tag{3}$$

where T_{g} is the average gas temperature in the TC (K), $h_{\text{g-c}}$ is the heat transfer coefficient between gas and the cryocooler ($\mathrm{W \cdot m^{-2} \cdot K^{-1}}$), A_{c} is the area of the cryocooler heat exchanger surface ($\mathrm{m^2}$).

II.2.3 Steady-state for the atmosphere and the gas in the thermal chamber

$$q_{\mathrm{L}} = \frac{T_{\mathrm{atm}} - T_{\mathrm{g}}}{R_{\text{atm-g}}} = \frac{T_{\mathrm{atm}} - T_{\mathrm{g}}}{\frac{L_{\mathrm{w}}}{k_{\mathrm{w}} A_{\mathrm{w1}}} + \frac{1}{h_{\mathrm{w2}} A_{\mathrm{w2}}}} \tag{4}$$

where q_{L} stands for the leaks of parasitic heat inflows (W). The total thermal resistance of the system "atmosphere-gas" $R_{\text{atm-g}}$ includes: 1) thermal resistance of the TC wall defined by the thickness L_{w} (m), the heat conductance k_{w} ($\mathrm{W \cdot m^{-1} \cdot K^{-1}}$), and the external freezing chamber surface area A_{w1} ($\mathrm{m^2}$) and 2) the thermal resistance between the internal freezing chamber wall and the circulating gas. The latter is defined by the heat transfer coefficient between the wall and gas h_{w2} ($\mathrm{W \cdot m^{-2} \cdot K^{-1}}$) and the surface area of the internal freezing chamber wall A_{w2} ($\mathrm{m^2}$).

II.2.4 Steady-state gas temperature in the thermal chamber

In the steady-state, the gas temperature inside the TC is constant because the heat flow rate created by heat pumping from the TC is compensated by the parasite heat flow rate from the atmospheric environment.

$$q_{\mathrm{c}} = q_{\mathrm{L}} \tag{5}$$

Using equations 3, 4 and 5 we find T_{g} :

$$T_{\text{g}} = \frac{T_{\text{atm}} \cdot R_{\text{g-c}} + T_{\text{c}} \cdot R_{\text{atm-g}}}{R_{\text{g-c}} + R_{\text{atm-g}}} \tag{6}$$

Using equations 1 and 3 we find T_{c}:

$$T_{\text{c}} = \frac{T_{\text{g}}}{R_{\text{g-c}} \cdot S_{\text{c}} \cdot \Theta \cdot f \cdot p \cdot \frac{1}{T_{\text{r}}} + 1} = \frac{T_{\text{g}}}{R_{\text{g-c}} \cdot \Theta \cdot \text{C} + 1} \tag{7}$$

Combining equations 6 and 7 we obtain steady-state gas temperature in the TC, $T_{\text{g}}^{\text{st.s}}$:

$$T_{\text{g}}^{\text{st.s}} = \frac{T_{\text{atm}} \cdot R_{\text{g-c}}}{R_{\text{atm-g}} + R_{\text{g-c}} - \frac{R_{\text{atm-g}}}{R_{\text{g-c}} \cdot \Theta \cdot \text{C} + 1}} \tag{8}$$

II.3 Calculation of thermal resistances

To calculate the steady-state temperature in Eq. 8, one needs to calculate the thermal resistances $R_{\text{g-c}}$ between the gas and the SC and between the atmosphere and the gas in the cooling chamber, $R_{\text{atm-g}}$.

II.3.1 Thermal resistance between the gas and the Stirling cryocooler

We first calculated the heat transfer coefficient between gas and the cryocooler $h_{\text{g-c}}$. The cold surface of the SC is a bank of plain tubes. Therefore, we used a classical approach to calculate $h_{\text{g-c}}$ from Gnielinski *et al.* (1983). For this calculation, one needs to know the geometry of heat exchangers, the table properties of the gas in the TC and its main flow velocity. We measured the geometry directly, used the table properties for air, and obtained the gas velocity in the chamber experimentally. To find the main flow velocity, we conducted three measurements in six different locations of the TC using the CEM DT-318 Flexible thermo-anemometer with the accuracy ±3% and averaged the measurements.

II.3.2 Thermal resistance between the atmosphere and the gas

The thermal resistance of the chamber wall has had a varying thickness, and we used the average value $L_{\mathrm{w}} = 62\ \mathrm{mm}$. The wall consisted of different types of isolation materials; therefore, the heat conductance of the wall material was averaged by thickness and was equal $k_{\mathrm{w}} = 0.04\ \mathrm{W \cdot m^{-1} \cdot K^{-1}}$. The external TC surface area was $A_{\mathrm{w1}} = 0.724\ \mathrm{m^2}$. To calculate thermal resistance between the internal chamber wall with $A_{\mathrm{w2}} = 0.259\ \mathrm{m^2}$ and the gas in the chamber, one needs to calculate the heat transfer coefficient h_{w2}. To do so, we used a classical relation to find the Nusselt number for a turbulent flow, because the value of $\mathrm{Re}_{\text{w2-g}} = 14000$:

$$\mathrm{Nu}_{\text{w2-g}} = 0.037 \cdot \mathrm{Re}_{\text{w2-g}}^{4/5} \cdot \mathrm{Pr}_{\text{w2-g}}^{1/3} \tag{9}$$

II.4 Evaluation of model accuracy

We selected three accuracy metrics to evaluate how reliably the developed model predicts temperatures compared to experimental measurements. These metrics are the coefficient of variance, mean biased error, and coefficient of determination.

The coefficient of variance (CV) given below:

$$\mathrm{CV} = \frac{\sqrt{\frac{1}{n-1}\sum_{i=1}^{n}\left(x_i - \hat{x}_i\right)^2}}{\overline{x}_i} \cdot 100 \tag{10}$$

is the average magnitude of the error. It shows the average difference between what the model predicted and what was measured in a real experiment. This parameter does not account for the sign of those differences (square). As it penalizes more significant errors because of the quadratic form, the smaller the CV, the better the prediction. In Eq. 10, *n* is the number of experimental points corrected with the Bessel's correction ($n-1$ instead of n), x_i is the measured parameter value, $\hat{x}_i$ the predicted parameter value, and $\overline{x}_i$ the mean value of the measured parameter. In this work, x_i takes values of $T_{\mathrm{g}}^{\mathrm{st.s}}$ and T_{c}.

The mean biased error:

$$\mathrm{MBE} = \frac{1}{n-1} \cdot \frac{\sum_{i=1}^{n} \left(x_i - \hat{x}_i \right)}{\overline{x}_i} \cdot 100 \tag{11}$$

characterizes the average magnitude of a systematic error. Unlike for CV, similar positive and negative errors in MBE would cancel each other out. The smaller the MBE, the less systematic errors in the model. The coefficient of determination (R^2) in Eq. 12 shows how the squared prediction error of the proposed model (nominator) is related to the squared prediction error of the model that always predicts the mean value of measurements (denominator). It ranges from 0 to 1, where 0 means the worst fit and 1 means the perfect fit.

$$R^2 = 1 - \frac{\sum_{i=1}^{n} \left(x_i - \hat{x}_i \right)^2}{\sum_{i=1}^{n} \left(x_i - \overline{x}_i \right)^2} \tag{12}$$

For good accuracy, CV and $\left|\mathrm{MBE}\right|$ should be no more than 5% and R^2 no less than 0.95.

II.5 Experimental measurements of the steady-state temperature

Experiments aimed to measure the steady state temperature in the TC of a real SC for different charge pressures and shaft frequencies. The results of experiments were used to validate the numerical model for a wide range of operational parameters.

II.5.1 Stirling cryocooler test rig

The principal diagram and the external view of the SC test rig is depicted in Fig. 2.

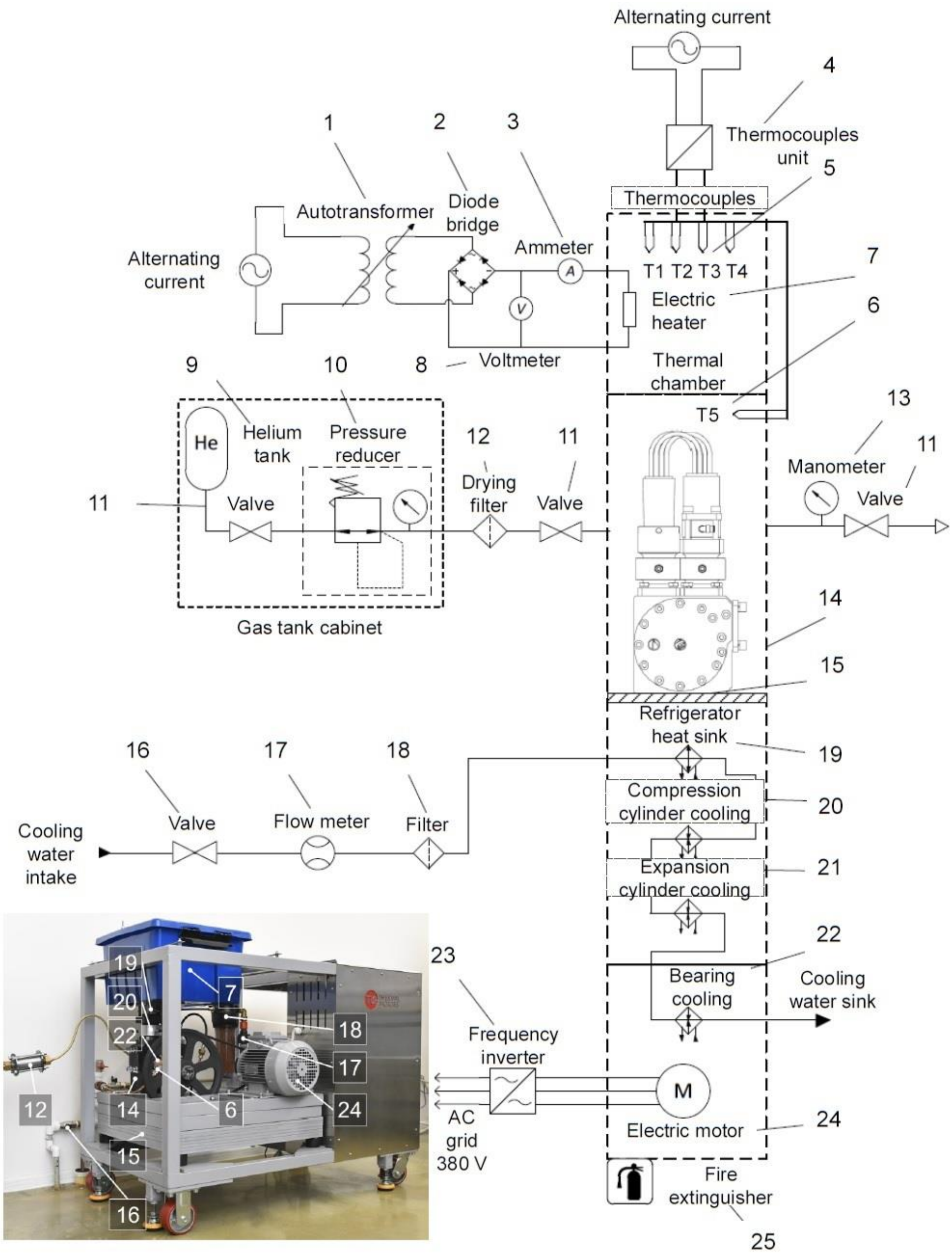

Fig. 2. Principal diagram and external view of the in-house Stirling cryocooler test rig.

Key sub-systems included: the helium supply system, positions (9)–(13), the cooling water supply system, positions (16)-(22), the electric motor system, positions (23) and (24), the temperature measurement system, positions (4) and (5), and the electrical heating system, position (1)–(3), (7) and (8). Table 3 summarizes the values of the parameters measured in the test rig with information about the accuracy of the measurements.

Table 3. Measured parameters and instruments in the in-house Stirling cryocooler test rig.

Parameter	Unit	Accuracy	Fig. 1	Instrument
Cooling temperature, T_c	°C	±0.25%	5 (T1)	Thermocouple Chromel Alumel (K), −270°C…1372°C
Temperatures: ambience T_a, cooling water T_h, bearing system T_b	°C	±0.25%	5 (T2, T3, T4), 6 (T5)	Thermocouple Chromel Alumel (K), −200°C…780°C
Charge pressure p,	MPa	±2.5%	13	Manometer YAFU 4.0 MPa
Shaft frequency f	rpm	±0.05%	Not shown	Digital tachometer Sinometer DT2234B
Cooling water flow rate, $\dot{m}_c$	$\mathrm{l \cdot s^{-1}}$	±5%	17	Digital flow meter Gardena 8188

II.5.2 Preliminary test

The electrical heating load in this work is set to zero. The resulting q_c consists of parasitic heat inflows from the environment. Although q_c was not measured directly in this case, it was calculated from measured parameters and empirical law: $q_c = A_c h_{\text{c-g}} \left(T_g^{\text{s.st}} - T_c \right)$. Three independent tests were carried out at nominal parameters of the SC— $p = 2.5\,\mathrm{MPa}$, $f = 550\,\mathrm{rpm}$ and $m_c = 5\,\mathrm{l \cdot min^{-1}}$—to obtain experimentally the Otaka number Θ as the arithmetic average. The constant was used in Eq. 7 to predict the steady-state gas temperature at different operational parameters of the SC.

II.5.3 Test methodology

The measurements comprised 13 separate tests at different non-nominal operational parameters of the SC. During each test the SC was operated at different charge pressures and shaft frequencies. For charge pressures 0.5 MPa and 1.5 MPa the SC operated at 110 rpm, 220 rpm, 330 rpm, 440 rpm and 550 rpm. For pressure 2.5 MPa the shaft frequencies were 110 rpm, 440 rpm and 550 rpm. At frequencies 220 rpm and 330 rpm the electrical motor was overheating due to non-optimal operational points and high compression forces. The objective of each test was to reach the condition in the TC, at which the change of gas temperature was less than 0.5 degree/minute. Although this condition does not represent an ideal steady-state, it helped to reduce the experiment time and find a state where the temperature does not change significantly over time. This temperature represented a quasi-steady state. Preliminary tests with longer operation times demonstrated that after the quasi-steady state is reached, the further temperature change was less than 5 K, an acceptable discrepancy in experimental results.

The quasi-steady-state temperature $T_{\mathrm{g}}^{\mathrm{st.s}}$ was measured using two thermocouples. One was installed in the upper part of the TC and the other in the lower part (Fig. 2, T3 and T4). The resulting value was the average between two measurements. The temperature of the SC T_{c} was also measured with two thermocouples (Fig. 2, T1 and T2) at the cold heat exchanger (Fig. 1a) and the resulting temperature was an arithmetic average.

III Results

III.1 Preliminary tests

The gas that moved around the bank of tubes had the average velocity of 1 $\mathrm{m \cdot s^{-1}}$. Around the walls, gas had the average velocity of 0.7 $\mathrm{m \cdot s^{-1}}$. Thermal resistances were calculated using average values of the air thermal properties in for temperatures between 193 K and 273 K, $R_{\mathrm{g\text{-}c}} = 0.771\,\mathrm{K \cdot W^{-1}}$ and $R_{\mathrm{atm\text{-}g}} = 2.687\,\mathrm{K \cdot W^{-1}}$.

Table 4 shows measurement results for the three preliminary tests, cooling capacity and the Otaka number.

Table 4. Measurement and calculation results for three preliminary tests.

Test number	p, MPa	f, Hz	T_{r}, K	$T_{\mathrm{g}}^{\mathrm{st.s}}$, K	T_{c}, K	q_{c}, W	Θ calculated, Eq. 1
1	2.5	8.9	289	168	123	56.6	0.059
2	2.5	8.9	287	169	129	50.2	0.052
3	2.5	8.9	287	162	128	43.3	0.048

Although the maximum variations of values for $T_g^{st.s}$ and T_c is 7 K or 5%, the resulting maximum variation in cooling capacity is significant, 13.3W or 30%. Different measured temperatures are the result of different initial operating conditions. In Tests 1 and 2, the SC was in thermal equilibrium with the atmosphere before the launch, and it took 40 minutes before reaching the quasi-steady state in both tests. However, before Test 3, the SC had worked for 45 minutes, and the system was in a precooled condition; therefore, the time required to reach the quasi-steady state was less than in Test 1 and 2, 15 min. Time constraints and other practical limitations did not allow to carry out Tests 1, 2, and 3 on the same day; therefore, they were conducted on different days. This approach affected the cooling water temperature and the thermal state of the system. The ambient temperature in the room was controlled with a thermostat and was constant at 297 K. These differences in initial conditions influenced the temperature measurements. On the other hand, this variation better represented the operation in a real environment and helped calculate a more realistic average Otaka number, which from Table 4 was equal to 0.053.

III.2 Experimental measurements

Table 5 lists the experimental data. Fig. 3 shows the comparison between experimental and calculated temperatures $T_g^{st.s}$ and T_c with the assumption of a constant Θ. The model demonstrated an unacceptable performance with CV=14%, MBE=–12% and $R^2 = 0.61$. The only input parameter in the model that has not been measured or controlled during the experiment was the Otaka number. Therefore, we manually adjusted the number to match the SC temperature measured in the experiment.

Table 5. Measurement results

Test number	$T_g^{st.s}$, K	T_c, K	p, Pa	f, Hz	T_r, K	q_c, W
1	281	272	0.5	1.8	287	11.7
2	258	245	0.5	3.7	287	16.9
3	237	221	0.5	5.5	287	20.8
4	220	202	0.5	7.3	287	23.3
5	206	186	0.5	9.1	287	25.9
6	246	232	1.5	1.8	287	18.2
7	220	198	1.5	3.5	287	28.5
8	199	171	1.5	5.3	287	36.3
9	176	147	1.5	7.2	287	37.6
10	167	136	1.5	9	287	40.2
11	248	226	2.5	2	287	28.5
12	176	144	2.5	6.5	287	41.5

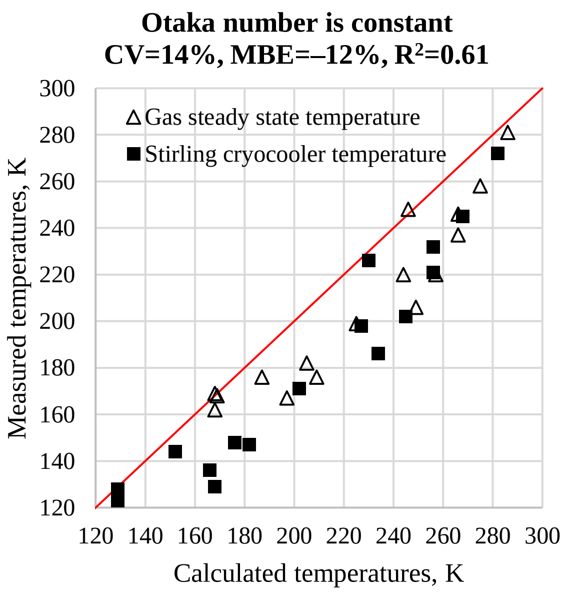

Fig. 3. Measured and calculated temperatures in the thermal chamber with a constant Otaka number.

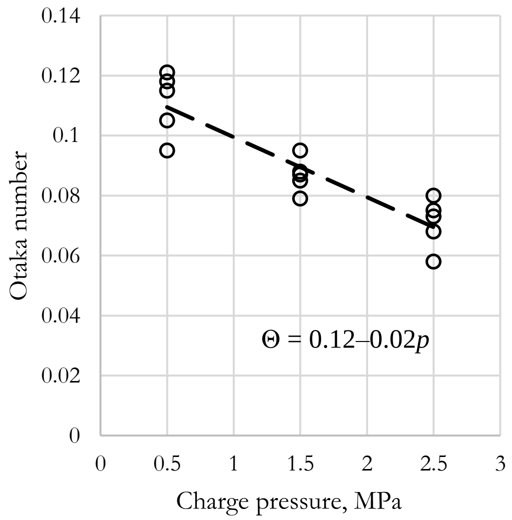

Fig. 4. Relationship between Stirling cryocooler charge pressure and the Otaka number

Then we analyzed the effect of each controlled parameter for the SC on resulting Θ. The charge pressure p was the only variable with strong influence. The relation for $\Theta = f(p)$ where δ is a cryocooler design constant reads:

$$\Theta = \delta - 0.02p \tag{13}$$

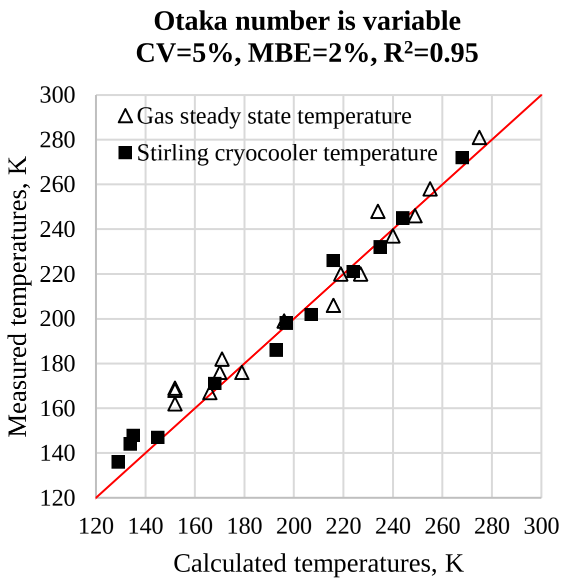

Fig. 5. Measured and calculated temperatures in the thermal chamber with a variable Otaka number.

Table 6. Experimental data for Stirling coolers in literature

Reference	**Cooler type**	**Frequency, Hz**	**Charged pressure, MPa**	**Hot side temperature, K**	**Cold side temperature, K**	**Cooling capacity, W**	$\Theta \cdot S_c$, **cm^3 calculated**
Otaka *et al.* (2002)	Kinematic beta, He	16.7	0.7	303	233	100	11.1
Lean et al. (2009)	Kinematic alpha, He	13.3	1.2	n/a (293 assumed)	238	70	5.4
Batooei & Keshavarz (2018)	Kinematic gamma, He	8.6	0.5	291	180	68	25.5
Djetel-Gothe *et al.* (2020)	Kinematic Beta, N	12.1	1.75	283	273	550	26.9
This study	Kinematic alpha, He	8.9	2.5	293	129	50	5.1

The relation is noteworthy. Otaka's number is not constant as it was put forward by Otaka *et al.* (2002) and initially assumed in this work. The results indicate that with higher charge pressure, the performance of the SC, which is characterized in Eq. 1 by Θ, declines. The linear relation in Fig. 4 was used to calculate the Otaka number in Eq. 8. The results are depicted in Fig. 5.

Let us formulate a general recommendation to choose the value of δ for first-order estimations during the SC design. Table 6 shows data for experimental SCs analyzed in the literature. The last column uses the data and Eq.1 to calculate the product of $\Theta \cdot S_c$. This parameter defines the effects of a particular cooler design and other efficiency-related factors. It ranges from 5.1 to 26.9 and plays only an *indicative* role here. These Stirling machines are different; therefore, this range serves for first-order estimations. To estimate δ, one should:

1) make early design decisions to estimate the value for S_c, Eq. 2;
2) using Table 6, select the value from $\Theta \cdot S_c = 5.1...26.9$, which is the closest to selected design decisions;
3) find Θ; and
4) calculate δ using the selected nominal charge pressure p_{nom}, $\delta = \Theta + 0.02 \cdot p_{nom}$.

The result would give some initial estimation of δ for the relation between the Otaka number and charge pressure.

III.3 Model accuracy

For the model with a constant Θ (Fig. 3), the coefficients of variation for $T_g^{st.s}$ and T_c are 12% and 16%, and the coefficients of determination are 0.6 and 0.62. This level of accuracy is not acceptable. It is evident that the model systematically and, in some instances, quite significantly overestimated the objective temperatures. This is also confirmed by the corresponding mean bias errors of −10% and −14%. The model predicted temperatures significantly higher than was measured in the experiment for the same input parameters. This means that the modelled SC is less efficient than the one in the experiment mainly because of a systematic error of constant Θ.

For results in Fig. 5, the Otaka number was corrected using the linear fitting line in Fig. 4. The coefficients of variation are 4% and 5%, the mean bias errors of −2% and −3%, and the coefficients of determination are 0.94 and 0.96 for $T_{\mathrm{g}}^{\mathrm{st.s}}$ and T_{c} correspondingly. These values represent a significant and satisfactory improvement of the model accuracy.

IV Discussion and concluding remarks

This work had two objectives:

1) To develop a unified numerical model for the system “Stirling cryocooler – Thermal chamber" to predict the steady-state temperature of the gas in the chamber.

2) To carry out experimental tests to collect temperature data and validate the prediction accuracy by a developed analytical relation.

Both objectives were reached. The results of the experiments helped improve the accuracy of the initial analytical relation, Eq. 7, by uncovering the systematic error in the original assumption of constancy of the Otaka number. The data demonstrated the relation between the Otaka number and cryocooler charge pressure. The main result can be summarized with this formula:

$$T_{\mathrm{g}}^{\mathrm{st.s}} = \frac{T_{\mathrm{atm}} \cdot R_{\mathrm{g\text{-}c}}}{R_{\mathrm{atm\text{-}g}} + R_{\mathrm{g\text{-}c}} - \dfrac{R_{\mathrm{atm\text{-}g}}}{R_{\mathrm{g\text{-}c}} \cdot \mathrm{C} \cdot \left(\delta - 0.02p\right) + 1}} \tag{14}$$

The recommendations to make an initial estimation of δ were also provided. The novelty of this result is that it unified and experimentally verified the relation for the joint operation of a SC and a TC. It is an important first step to fully define and control the cryogenic environment as a function of *controllable* design variables of the cryocooler and TC. Inventions, discoveries and technological products would increasingly originate from cryogenic spaces. Therefore, it is vital to learn how to control them with electricity and engineering tools (such as electrical cryocoolers). Apart from design, the relation above could be utilized in control algorithms.

The history of Stirling machines shows that academic work most of the time has followed the activities in the industrial sector (Smirnov & Willoughby, 2021). Similar results of predicting temperatures could already be found and utilized by companies. A notable example is the Asymptote's Stirling cryocooler-controlled chambers (Whale, 2017). However, the details of commercial technology are often hidden under the veil of trade secrecy. In this work, we experimentally explored the coupling between a SC and a TC giving an unprecedented wealth of details. In addition, other promising topics would always pose the need for basic understanding of the coupling. The recent interest in cryo-CMOS electronics with the advent of quantum computers serves a good example (Smirnov & Ouerdane, 2021).

The empirical relation factored out the most problematic variable in similar design problems—the temperature of the cryocooler. First, the cryocooler temperature is subject to cryocooler design. One can select a desirable temperature, but the real physics inside the assumed design characterized by Θ would render this selection moot. Second, the temperature is the result of thermal balance. Conventional thinking tells that the Stirling cycle operates between two isotherms, and one should simply select their values. Indeed, we can safely assume that the hot isotherm T_r is constant because cooling water or room environment can play the role of a large heat sink. But the cold isotherm is a delicate balance between the cryocooler and TC design. The advantage of the relation above is that it includes only *controllable* parameters of the system with the exception of δ, which is an empirical constant taken from the literature.

IV.1 Limitations

The primary limitation is the need to know δ (Eq. 13)—an empirical characteristic of the cryocooler design performance—before estimating the steady-state temperature of the gas in the chamber. Although we provided some recommendations to make a first-order estimation of δ, predicting the performance of a machine as complex as the SC is an arduous task. However, alternative ways appear to be more challenging. A full mathematical model accounting for all the physical phenomena in the cryocooler and its coupling with the cryogenic chamber seems out of reach as obtainment of a tractable closed-form solution considering the complex boundary conditions would be extremely difficult nay impossible. Numerical modelling might be a part of the solution; however, these models need a basic theoretical ground as a "starting point". Typically, this starting point is provided by first-order estimations. Our result offers some initial guidance for these estimations. With more experimental data on SCs, chances to describe the complexity of these machines using simple empirical coefficients increase. However, such a result would require more effort to generalize the findings of empirical research and conceptualize them into dimensionless numbers that others in the field can use. This work is also not devoid of limited generalization of experimental data. However, we hope that the general empirical formula (Eq. 14) would contribute to fill this gap.

Results offer an initial relation to estimating the Otaka number. The assumption that *the slope defined by coefficient 0.02 would hold for other designs of cryocoolers* needs further validation. On the other hand, the relation between energy conversion performance and charge pressure for the reversed Stirling cycle might be less dependent on a particular design. Rather, the slope is defined by fundamental limitations of thermodynamic systems to be efficient and pump more heat at the same time (Andersen et al., 1984). As such, the coefficient of 0.02 should give an approximate slope, not completely off the mark. The coefficient should be studied for a more extensive range of pressures using different configurations of cryocoolers to establish a more accurate value of the coefficient or the form of the relation.

Figure 4 also revealed that the Otaka number depends on other parameters, for example, frequency. The data collected in this work could not be used to derive the relation between

Otaka number and frequency conclusively. Otaka et al. (2002) described the effects of a cryocooler temperature on the Otaka number. However, this relation is difficult to implement, as the temperature is a dependent variable and cannot be controlled. This limitation can be addressed in a dedicated future work.

IV.2 Future Work

Equation 5 is a steady-state condition for cryocooler and parasitic heat inflows. There was no other controlled heating load (i.e. electrical heater) in the chamber. The next steps should include an analytical definition and experimental validations of the following conditions:

1) $q_c = q_L + q_R$, where q_R is a heat flow from thermal radiation;
2) $q_c = q_L + q_R + q_S$, where q_S is a heat flow from a constant heat source;
3) Transient conditions. Some work in this direction has been done by Hachem et al. (2017), which focused on the transient processes within the cryocooler;
4) Improving the accuracy of predicting the Otaka number (Eq.13).

V Conclusions

- We developed a numerical model for the system "Stirling cryocooler – thermal chamber" based on the electrical-thermal analogy and previously established Otaka's equation of the Stirling cryocooler to predict the steady-state temperatures in the chamber.
- We conducted a series of 15 tests of the real alpha-type Stirling cryocooler at mean pressures ranging from 0.5 MPa to 2.5 MPa and shaft frequencies ranging from 110 rpm to 550 rpm. Collected experimental data for the range of temperatures from 272 K to 128 K and cooling capacities from 10 W to 53 W. The data was used to validate the model.

- We obtained an empirical relation for the Otaka number (cryocooler efficiency) as a linear function from cryocooler charge pressure. The relation substantially increased the accuracy of the model prediction.
- The coefficient of variance for the predicted temperature of circulating air in the chamber is 4%, for the cryocooler temperature is 5%. The mean bias error is −2% and −3%, the coefficient of determination is 0.94 and 0.96.

References

Andresen, B., Salamon, P. and Berry, R.S. (1984) 'Thermodynamics in finite time', *Physics today*, 37(9) p.62. Available at: https://doi.org/10.1063/1.2916405.

Batooei, A. and Keshavarz, A., (2018) 'A Gamma type Stirling refrigerator optimization: An experimental and analytical investigation', *International journal of refrigeration*, 91, pp.89-100. Available at: https://doi.org/10.1016/j.ijrefrig.2018.05.024.

Djetel-Gothe, S., Bégot, S., Lanzetta, F. and Gavignet, E. (2020) 'Design, manufacturing and testing of a Beta Stirling machine for refrigeration applications', *International Journal of Refrigeration*, 115, pp.96-106. Available at: https://doi.org/10.1016/j.ijrefrig.2020.03.005.

Gnielinski, V., Zukauskas, A., and Skrinska, A. (1983) 'Fluid mechanics and heat transfer. Single-phase convective heat transfer. Banks of plain and finned tubes', *Heat exchanger design handbook*, Vol. 2, p.460. Hemisphere Publishing Corporation.

Hachem, H., Gheith, R., Aloui, F. and Nasrallah, S.B. (2017) 'Optimization of an air-filled Beta type Stirling refrigerator', *International Journal of Refrigeration*, 76, pp.296-312. Available at: https://doi.org/10.1016/j.ijrefrig.2017.02.019.

Kirk, A.C. (1874) 'On the mechanical production of cold', In *Minutes of the Proceedings of the Institution of Civil Engineers* , 37, No. 1874, pp. 244-282. Available at: https://doi.org/10.1680/imotp.1874.22807.

Kwon, Y.R. and Berchowitz, D.M.(2003) 'Operational characteristics of Stirling machinery', *International Congress of Refrigeration* , 8.

Le'an, S., Yuanyang, Z., Liansheng, L. and Pengcheng, S. (2009) 'Performance of a prototype Stirling domestic refrigerator', *Applied Thermal Engineering, 29(2-3),* pp.210-215. Available at: https://doi.org/10.1016/j.applthermaleng.2008.02.036.

Lienhard, J.H. IV and Lienhard, J.H. V (2001) *A heat transfer textbook*, 3rd edition, Cambridge, MA: Leinhard

Oguz, E. and Ozkadi, F. (2000) 'An Experimental study on the refrigeration capacity and thermal performance of free piston stirling coolers', *International Refrigeration and Air Conditioning Conference,* paper 520. Available at: http://docs.lib.purdue.edu/iracc/520.

Oguz, E. and Ozkadi, F. (2002) ‘Experimental investigation of a stirling cycle cooled domestic refrigerator’, *International Refrigeration and Air Conditioning Conference*, paper 623. Available at: http://docs.lib.purdue.edu/iracc/623.

Otaka, T., Kodama, I. and Ota, M. (2008) ‘Experimental study on a Stirling cycle machine of 100W design capacity’, *Journal of Power and Energy Systems*, 2(3), pp.1027-1035. Available at: https://doi.org/10.1299/jpes.2.1027.

Otaka, T., Ota, M., Murakami, K. and Sakamoto, M. (2002) ‘Study of performance characteristics of a small Stirling refrigerator’, *Heat Transfer—Asian Research: Co‐sponsored by the Society of Chemical Engineers of Japan and the Heat Transfer Division of ASME*, 31(5), pp.344-361. Available at: https://doi.org/10.1002/htj.10033.

Rafique, M.M.A. (2015) ‘Modeling and Simulation of Heat Transfer Phenomena’ in Kazi, S.N. (ed.) *Heat Transfer Studies and Applications*. IntechOpen. Availiable at: https://doi.org/10.5772/58727

Smirnov, D. and Ouerdane, H., (2021) The operation of the CMOS device at different frequencies under various cooling conditions. *Unpublished manuscript.*

Smirnov, D., Dvortsov, V., Saichenko, A., Tkachenko, M., Kukolev, M., Bischi, A. and Ouerdane, H. (2019) ‘Experimental study of a high-tolerance piston-cylinder pair in the alpha Ross-yoke Stirling refrigerator’, *International Journal of Refrigeration*, 100, pp.235-245. Available at: https://doi.org/10.1016/j.ijrefrig.2019.01.018.

Smirnov, D.S. and Willoughby, K.W. (2021) ‘Rethinking the dynamics of innovation, science, and technology: The curious case of Stirling engines and Stirling refrigerators’, *Energy Research & Social Science*, *79*, p.102159. Available at: https://doi.org/10.1016/j.erss.2021.102159.

Whale, T.F., Holden, M.A., Kulak, A.N., Kim, Y.Y., Meldrum, F.C., Christenson, H.K. and Murray, B.J. (2017) ‘The role of phase separation and related topography in the exceptional ice-nucleating ability of alkali feldspars’, *Physical Chemistry Chemical Physics*, 19(46), pp.31186-31193. Available at: https://doi.org/10.1039/C7CP04898J.